

ANISE: Assembly-based Neural Implicit Surface rEconstruction

DMITRII PETROV*, University of Massachusetts Amherst, USA

MATHEUS GADELHA, Adobe Research, USA

RADOMÍR MĚCH, Adobe Research, USA

EVANGELOS KALOGERAKIS, University of Massachusetts Amherst, USA

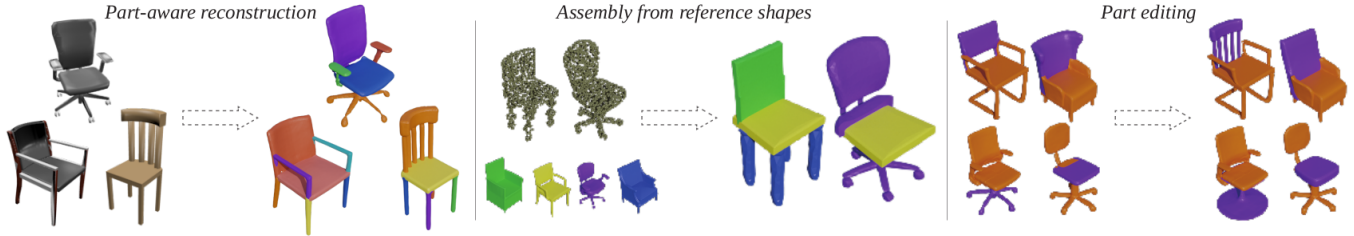


Fig. 1. We introduce a shape representation for 3D reconstruction through a set assembly of neural implicits (**left**). Our approach results in state-of-the-art reconstruction quality. It can also perform reconstruction constrained on a database of reference parts or shapes (**middle**) – the model here uses only shapes provided by the user. Finally, it allows part-level editing of outputs (**right**).

We present ANISE, a method that reconstructs a 3D shape from partial observations (images or sparse point clouds) using a part-aware neural implicit shape representation. It is formulated as an assembly of neural implicit functions, each representing a different shape part. In contrast to previous approaches, the prediction of this representation proceeds in a coarse-to-fine manner. Our network first predicts part transformations which are associated with part neural implicit functions conditioned on those transformations. The part implicit functions can then be combined into a single, coherent shape, enabling part-aware shape reconstructions from images and point clouds. Those reconstructions can be obtained in two ways: (i) by directly decoding combining the refined part implicit functions; or (ii) by using part latents to query similar parts in a part database and assembling them in a single shape. We demonstrate that, when performing reconstruction by decoding part representations into implicit functions, our method achieves state-of-the-art part-aware reconstruction results from both images and sparse point clouds. When reconstructing shapes by assembling parts queried from a dataset, our approach significantly outperforms traditional shape retrieval methods even when significantly restricting the size of the shape database. We present our results in well-known sparse point cloud reconstruction and single-view reconstruction benchmarks.

1 INTRODUCTION

Neural implicit surface representations have gained increasing popularity for 3D reconstruction due to their ability to model shapes as continuous surfaces without topology restrictions. Despite their advantages, they also have shortcomings. Most existing approaches are agnostic to part structure. This contrasts the observation that most man-made objects are compositional i.e., they are made out of parts. As a result, they often end up producing surfaces with implausible part arrangements. In addition, their outputs are far from being controllable. For example, if users want to edit parts in the output shape they need to perform post-processing segmentation steps, which can further amplify errors during editing.

We propose ANISE, a new *part-aware* shape reconstruction method based on neural implicits. Specifically, given a partial shape observation (image or point cloud), it reconstructs shapes as a combination of parts, each with its own geometric and structural representations. We propose assembling those parts in two different manners: as a union of part implicit functions, or by retrieving similar parts in a part database. The former generates well-connected shapes without gaps or self-intersections whereas the later perfectly preserves the quality of the parts in the reference set, providing more control over the reconstruction process. Regardless of the way the parts can be assembled, our method can be trained and tested on shapes with varying number of parts i.e., we do not assume a fixed number of parts, and impose only an upper bound on their number.

A key feature of our approach is that it explicitly *disentangles geometry from structure*. Instead of forcing the network to learn how to predict the whole surface at once, we decompose this task into these two simpler learning problems representing a coarse-to-fine shape reconstruction. More specifically, our model first reconstructs a structural arrangement of the shape in the form of geometric transformations of its parts. Conditioned on them, the model predicts a neural implicit function tailored for each part. Our experiments demonstrate more accurate surface reconstructions compared to previous neural implicit methods that model the surface as a whole.

Another important property of ANISE is that it does not impose any particular order over the shape parts, which tends to be ambiguous in the case of 3D shapes. This contrasts the recent part-aware approach of PQ-Net [Wu et al. 2020], which assembles shapes using neural implicits for parts, but relying on a recurrent network trained on a sequence of parts in a particular order. For example, when compared to PQ-Net in a single-view reconstruction setting, our method increases the F-Score by at least 16.8%. Finally, our part retrieval and assembly approach establishes a new state-of-the-art for retrieval-based single-view reconstruction. Compared to previous approaches, our method requires shape databases *an order of magnitude smaller* to achieve the same reconstruction quality.

*Part of the work was done as Adobe Research internship.

We summarize our contributions as the following:

- A coarse-to-fine method to assemble a set of neural implicits. Unlike other part-based neural assembly methods, our method first predicts part transformations (cuboid approximations to parts), then predicts part geometry.
- A network architecture for assembling neural implicits, which can be fine-tuned end-to-end using supervision from full shapes instead of individual parts. This network significantly outperforms state-of-the-art methods for part-aware reconstructions (Tables 2 and 3).
- A simple yet surprisingly effective method for retrieving parts and assembling them to create new shapes matching a partial shape observation (image or point cloud). This part retrieval and assembly approach (PR&A) yields significant improvements over state-of-the-art shape retrieval and deformation counterparts (Table 2).

2 RELATED WORK

Learning implicit functions for 3D shape reconstruction. Several approaches have proposed employing implicit functions (or coordinate-based architectures) to represent 3D shapes [Chen and Zhang 2019; Mescheder et al. 2019; Park et al. 2019]. Those methods represent the surface of an object as the level-set of a function parametrized by a neural network. This function can be either seen as a binary classifier for occupied (or empty) regions of space [Chen and Zhang 2019; Mescheder et al. 2019] or a signed distance function (SDF) [Park et al. 2019; Xu et al. 2019]. Other techniques tried to improve the quality of the shapes represented by those functions through localized representations [Chabra et al. 2020; Genova et al. 2020; Jiang et al. 2020; Li and Zhang 2021; Paschalidou et al. 2021; Peng et al. 2020; Xu et al. 2019]. Similarly, other methods generate parameters of a fixed, previously defined implicit functions, either by predicting planes to generate convex polyhedra [Chen et al. 2020; Deng et al. 2020], directly estimating the weights of a smaller MLP [Littwin and Wolf 2019] or a set of radial basis functions [Genova et al. 2019]. Despite their quality, none of these models is designed to reason about meaningful shape parts; e.g. a particular component will not always represent the full leg of a chair, or the top of a table, or an engine of an airplane, and so on. Our work aims to describe shapes as an assembly of implicit functions parametrized by neural networks, where every function is responsible for generating a meaningful part. This allows users to perform part-aware shape operations, like editing specific elements and reconstructing shapes by assembling objects from pre-determined parts.

Part-based shape modeling. The seminal work by Funkhouser et al. [Funkhouser et al. 2004] employed user input for interactive segmentation and hand-crafted features for part exploration and shape composition. This synthesis-by-examples approach was later followed by techniques based on probabilistic models [Chaudhuri et al. 2011; Kalogerakis et al. 2012], evolutionary techniques [Xu et al. 2012], among others. Lately, several datasets with part annotations [Chang et al. 2015; Mo et al. 2019b] have allowed the development of less constrained and more automatic approaches

powered by deep neural architectures. A number of them are focused on generating solely structural information [Gadelha et al. 2020; Mo et al. 2019a; Zou et al. 2017].

More related to our approach are methods for generating the geometry of 3D parts and assembling them into a coherent shape. GRASS introduced a recursive neural network that represents shapes as binary part hierarchies whose leaves are decoded into geometric data [Li et al. 2017]. Dubrovina et al. [Dubrovina et al. 2019] proposed assembly-based neural shape modeling by first predicting voxelized parts, then part transformations through a spatial transformer. Li et al. [Li et al. 2020] proposed another voxel-based method for generating parts, then assembling them through regressed transformations. All these approaches rely on voxels and their high memory consumption limits their ability to reconstruct high-resolution shapes. Moreover, both Dubrovina et al. [Dubrovina et al. 2019] and Li et al. [Li et al. 2020] group part instances of the same *semantic* label (e.g., all chair legs) under the same transformation. ANISE, on the other hand, builds on top of implicit function representations (leading to more detailed shapes) and does not require semantic labels, producing one transformation for each part instance; e.g., each chair leg instead of a group of legs. Closely related to our work is the assembly-based neural implicit method by Wu et al. (PQ-Net). While their method also uses neural implicits as part representations, it generates parts and their transformations sequentially and, similarly to previous approaches, does not employ a coarse-to-fine generative procedure, which we demonstrate to be highly beneficial (Section 5.2). Moreover, our approach treats parts as sets instead of sequences, which simplifies the generation procedure — generating shapes with several parts accounts a single forward pass in our model. More importantly, we are able to obtain supervision from fully assembled shapes to fine-tune our model, leading to further qualitative and quantitative improvements. When combined, those characteristics lead to a significant improvement over PQ-Net in shape reconstruction from point clouds and single RGB images (Tables 2 and 3).

Shape retrieval. Another line of work related to ours consists of reconstructing shapes by retrieving similar ones from a database. The similarity measure is usually performed in some embedding space that encodes data of multiple modalities (e.g. point clouds, images, meshes), allowing the retrieval to be performed conditioned on various sources of data [Bell and Bala 2015; Li et al. 2015]. When compared to reconstruction approaches, retrieval counterparts offer the advantage of yielding high-quality shapes — stock models from shape repositories. On the other hand, the retrieved result might not be a good match for the data queried by the user. Previous works address this issue by exhaustively deforming the retrieved shape until it matches the target data [Nan et al. 2012] or by retrieving parametric models that can be better adjusted to the user query [Schulz et al. 2017]. More recently, Uy et al. proposed a joint retrieval and deformation model that is capable of deforming specific shape parts to enhance its similarity to the target data [Uy et al. 2021]. However, despite being able to deform parts independently, the model is still constrained to the retrieved shape. We derive a simple yet surprisingly effective part retrieval and assembly (PR&A) approach — use part latents and part transformations predicted by our model to

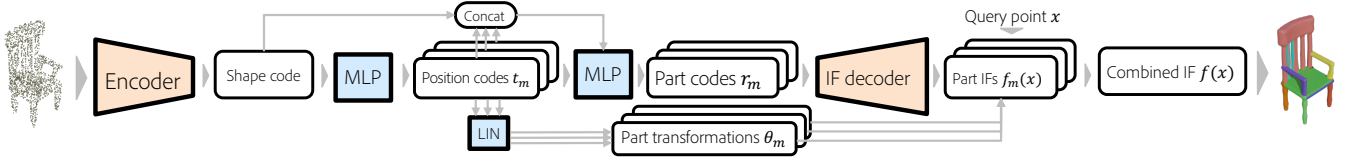


Fig. 2. **Network architecture.** ANISE takes a point cloud or RGB image as an input and outputs a neural implicit function evaluated at query point \mathbf{x} in 3D space. Our architecture starts with an input encoder which produces a global shape code. Based on this code, the network produces part transformation codes \mathbf{t}_m . From them and the shape code, the network predicts a set of part codes \mathbf{r}_m . These part codes are passed to an implicit function decoder along with the query points \mathbf{x} , which provides implicit functions for each part. Using the predicted transformations θ_m , these functions are transformed and combined into a complete shape implicit function.

retrieve similar parts in a database and correctly position assemble them. In other words, given a database of shapes and a partial shape observation (image or point cloud) our model is able to create a new shape by *combining parts from different shapes* in the database which closely match the partial observation. We show that our method significantly outperforms state-of-the-art retrieval and deformation approaches and is even able to do so by using shape databases with a fraction of the original size (Figure 7).

3 METHOD

An overview of our approach is depicted in Figure 2. It consists of three modules. The first module predicts a coarse part arrangement in the form of part transformations (“part transformation” module, Section 3.1). Then, conditioned on these part transformations, the next module predicts an implicit function representing the actual geometry (“part geometry module”, Section 3.2). The last module transforms each part implicit functions according to the predicted transformations and combines them into a single output implicit function $f(\mathbf{x})$ (“shape assembly module”, Section 3.3). This process can be thought as a coarse-to-fine surface prediction procedure, where shape is first predicted coarsely in the form of part transformations (e.g. placement, size, deformations, etc) to be later refined into fine geometry.

The network is trained with objectives that encourage both correct structure prediction and part geometry prediction based on a repository of segmented shapes (Section 4). Part labels are not required i.e., the segmentation does not need to be “semantic” but should be consistent across shapes. The whole architecture is trained to produce output implicit functions close to the ground-truth.

3.1 Part transformation module

This module takes as input observation \mathbf{O} , in the form of a single RGB image or sparse point cloud, and encodes it into a 256-dimensional shape code \mathbf{s} . This shape representation is then decoded by a MLP that produces M transformation codes. More specifically, the MLP implements a function $g(\mathbf{s}) = \{\mathbf{t}_m\}_{m=1}^M$, where \mathbf{t}_m is a 128-dimensional feature representation of the m^{th} part transformation. Each representation is then decoded into actual transformation parameters θ_m . In our experiments, we show that very simple transformations (just positioning and scale) are enough to produce shapes competitive to current state of the art approaches. From this aspect, these transformations can be thought of as predicting a cuboid – a coarse representation of each part.

It is important to note that the number M represents an upper bound of parts for the output shape ($M = 10$ in our experiments for all shape categories). During training, only a subset of the predicted transformations is matched with ground-truth ones, as discussed in Section 4. We note that we tried predicting an extra binary output representing the existence of a part, but it did not improve results. In practice, the network learns not to make use of extra parts i.e., they are decoded to implicits without zero crossings, or in other words, they are not filled with surface geometry, which counter-effects the need for such output parameter. We also note that the order of the predicted transformations does not matter since the subsequent modules of our architecture are invariant to part order. During training, the matching between predicted and training transformations is also order-insensitive.

3.2 Part geometry module

This module first takes as input the shape representation \mathbf{s} and each transformation representation \mathbf{t}_m and predicts a per-part geometric feature representation \mathbf{r}_m . This is done through M shared MLPs, each implementing the function $\mathbf{r}_m = h(\mathbf{t}_m, \mathbf{s})$. Then, an implicit surface decoder decodes each part’s feature representation \mathbf{r}_m to its implicit function $f_m(\mathbf{x}, \mathbf{r}_m)$. The zero level set of the function represents the surface of the part m . The module is trained to produce parts that are centered at the origin and scaled to have unit scale across axis with largest scale. This helps the decoder to focus on the geometry of parts, since their location and size are already captured in the part transformation module.

As discussed in Section 4, we found useful to decompose the prediction of the part implicit function into two stages (part feature representation prediction, then part implicit prediction) because this enables the ability to pre-train the implicit surface decoder that results in better performance. We also note that we tried other variants, such as predicting the part implicit functions without conditioning on part transformations, or skipping the part feature prediction part, yet these resulted in worse performance, as discussed in our experiments (see Table 4).

3.3 Shape assembly module

This module combines the part implicit functions into a single shape. We present two different approaches for accomplishing this task: part retrieval and assembly (PR&A), and implicit function assembly. The former retrieves parts from a database and assembles them using the predicted transformations, perfectly preserving the quality of

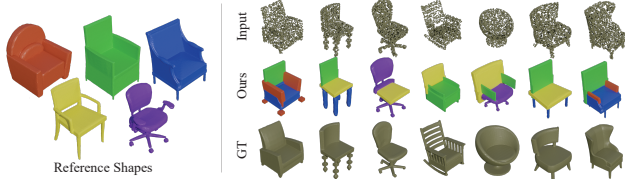


Fig. 3. **Part-constrained shape assembly.** Our model is capable of reconstructing sparse point clouds by assembling parts from a user-provided reference database of shapes or parts. In this example, the user selects 5 shapes (left) pre-segmented into parts. Our model reconstructs shapes that closely approximate the input point clouds while *only using parts from the reference shapes*. Differently from traditional shape retrieval-based methods [Bell and Bala 2015; Li et al. 2015; Uy et al. 2021] our approach can mix parts from different shapes to better approximate the target.

the assets on the database. The later allows the creation of more plausible connections between parts – since the process is fully differentiable we are able to fine-tune the assembly on complete shapes and improve part connections with the drawback of losing the exact correspondence to parts on a database.

Part retrieval & assembly (PR&A). For this approach, instead of using the implicit functions to generate geometry directly, we use the part latents ($\mathbf{r} \in \Gamma$) to query similar parts in a part database (also referred to as *reference set*). Let $\mathbf{Q} = \{\mathbf{q}_k\}_{k=1}^K$ be our part database, where K is their total number parts and \mathbf{q}_k is the geometric representation of the k -th part. Let $\phi(\mathbf{q}_k)$ be a function that projects the geometric part representation into Γ . Then, we can use the predicted part presentations \mathbf{r}_m to query a part $\hat{\mathbf{q}}_m$ such that $\hat{\mathbf{q}}_m = \arg \min_{\mathbf{q}_i \in \mathbf{Q}} \|\phi(\mathbf{q}_i) - \mathbf{r}_m\|_2$. The final shape can be assembled by transforming each part $\hat{\mathbf{q}}_m$ according to its predicted transformation θ_m . This approach has a couple of advantages. First, it is agnostic to the geometric representation – it can be applied as long as there is a way of computing a latent representation from its geometric one. This means that the final shape will keep the details and quality of the retrieved parts. Second, this can be used to provide the user of the system more control over the assembled shape by simply curating which parts will be present in the reference set (see Figure 3). A very important drawback of this approach comes from its first advantage. Since parts exactly correspond to the ones in the database, the connection between them might not be plausible. We propose to tradeoff the quality of the individual parts with the plausibility of the whole shape by also developing an alternative *implicit function assembly*, described in the next paragraph.

Implicit function assembly. We can also assemble complete shapes by combining the implicit function representation of the individual parts in a differentiable manner. The geometric union of implicit functions can be expressed using a minimum operation, after transforming the part according to the decoded transformation parameters θ_m .

$$f(\mathbf{x}) = \min_m T(f_m; \theta_m)(\mathbf{x}) \quad (1)$$

where T is a functional that transforms the implicit function f_m according to θ_m . The operation can be thought of as min pooling

over M part implicit functions modified with predicted transformations. Backpropagation through this operation enables learning part implicit functions such that their combination produces a coherent shape as a whole. For example, in case of a transformation θ_m consisting of part translation \mathbf{c}_m and uniform scaling α_m , implemented in our experiments, this formula can be written as [Museth et al. 2002; Reiner et al. 2011]:

$$f(\mathbf{x}) = \min_m \alpha_m f_m\left(\frac{\mathbf{x} - \mathbf{c}_m}{\alpha_m}\right) \quad (2)$$

where query point \mathbf{x} is transformed from shape centered space to a part centered and scaled space, thus allowing the evaluation of the part implicit function. In practice, we show that even this simple part transformation model is enough to achieve high reconstruction quality, surpassing state-of-the-art part-aware reconstruction approaches in various metrics. The scaling factor α_m in front of the implicit function is important to ensure that the scale of implicit functions hold after the union (e.g., in the case of scaling signed distance functions, distances should also be scaled [Museth et al. 2002; Reiner et al. 2011]).

4 TRAINING

We now describe the training procedure for ANISE. One possibility to train our architecture is to just provide a single supervisory signal in the form of target implicit function values obtained from ground-truth shapes. More specifically, given point samples $\{\mathbf{x}_i^{(p)}\}$ from \mathcal{R}^3 , where i is a point sample index and p is a training shape index, a common procedure in neural implicit fitting approaches [Chabra et al. 2020; Park et al. 2019; Xu et al. 2019] is to measure the signed distance $s_i^{(p)}$ of each point to the training shape’s surface, then minimize a loss between predicted implicit function values and signed distances: $\mathcal{L}_{shape} = \sum_{i,p} \mathcal{L}(f(\mathbf{x}_i^{(p)}), s_i^{(p)})$, where \mathcal{L} is set to L1 loss or clamped L1 loss [Xu et al. 2019]. Our architecture is fully differentiable, thus, this approach is entirely possible in our method. Unfortunately, it fails to deliver successful results: we observed that a single part is produced enclosing the whole training shape, while the rest collapse to negligible surfaces. As a result, no structure is captured from the network, and the performance of the method ends up being similar to structure-agnostic neural implicit methods.

We instead found that the best performance is achieved when we make use of shapes segmented into parts and then provide supervision in the form of part implicit functions, part transformations, and part feature representations. Thus, we follow a multi-stage training procedure described in the following paragraphs. First, we pre-train the part implicit decoder used in the part geometry module (Sec. 3.2). Second, we train the part arrangement and part geometry module together using supervision from part transformations and its feature representations. Finally, we fine-tune the whole network end-to-end using supervision from the implicit functions obtained from the complete shapes. The input to our training procedure is a set of shapes segmented into parts. We assume that the input shapes are consistently oriented. In our experiments, we make use of PartNet [Mo et al. 2019b], a popular repository of 3D meshes with part segmentations. Even though we make use of the shape segmentations, our training *does not* use their *semantic* labels.

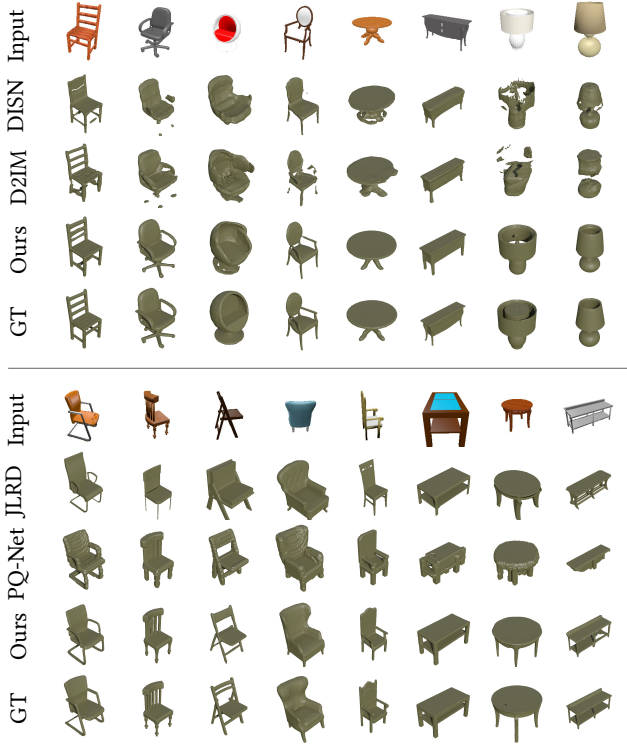


Fig. 4. **Single view reconstruction.** We compare with part-unaware methods (**upper block**) on ShapeNet and part-aware methods (**lower block**) on PartNet. Our model reconstructs fine details of the input like chair armrests or office chair swivel legs.

4.1 Pre-training stage

Our first stage involves pre-training the part implicit surface decoder f_m . The decoder is conditioned on the part geometric feature representation, thus, we need to generate those first for our training shapes. To achieve this, we train an encoder-decoder network that takes as input individual parts from the segmented training shapes, encodes them to a 256-dimensional descriptor in the bottleneck, then decodes them to part implicit functions. More specifically, given each training part, we center it to the origin and scale it uniformly such that the largest dimension of bounding box is one. In addition, since the mesh of the part often has holes at the part boundaries after excluding the rest of the shape, we reconstruct its mesh to a watertight version so that valid signed distance functions can be computed (more details in the supplementary material). Then we sample 10^5 points inside of bounding box of each part.

The encoder has the form of a PointNet [Qi et al. 2017] with skip connections that processes each part’s points. The output of the encoder is the feature representation of each part, denoted as $\hat{\mathbf{r}}_n^{(p)}$, where n is a training part index for a shape p . The decoder has the same architecture with our implicit surface decoder f_m in the part geometry module (Section 3.2). During training we add noise to part codes to make sure that representation space is smooth, so latent codes can be smoothly interpolated and the distance in this space corresponds to geometric similarity of parts.

The network is trained to minimize the L1 loss

$$\mathcal{L}_{part} = \sum_{i,p} \| (f_m(\mathbf{x}_i^{(p)}) - s_i^{(p)}) \|_1,$$

where $s_i^{(p)}$ is the target signed distance function value of the sample point $\mathbf{x}_i^{(p)} \in \mathcal{R}^3$ to the mesh part surface (details about sampling are provided in the supplementary material). The result of this stage is both a trained part implicit surface decoder f_m and geometry-encoding part features $\hat{\mathbf{r}}_n^{(p)}$ used in the subsequent stages.

4.2 Main training stage

We proceed with training our network using supervision from training part transformations and part feature representations. Specifically, for each training shape and part, we first extract an axis-aligned transformation with center position and scale parameters $\hat{\theta}_n^{(p)} = [\hat{c}_n^{(p)}, \hat{d}_n^{(p)}]$. We use isotropic scaling because it is compatible with SDF-based part assembly (see 3.3).

We use two losses to train our network. The first loss penalizes discrepancies between predicted transformation parameters and ground-truth ones. Specifically, given each predicted transformation m with parameters $\theta_m^{(p)} = [c_m^{(p)}, d_m^{(p)}]$ for each training shape p , our loss is expressed as follows:

$$\mathcal{L}_1 = \frac{1}{N_p} \sum_{n=1}^{N_p} \min_m \|\hat{\theta}_n^{(p)} - \theta_m^{(p)}\|_2 + \frac{1}{M} \sum_m \min_n \|\hat{\theta}_n^{(p)} - \theta_m^{(p)}\|_2 \quad (3)$$

where N_p is the number of training parts for shape p . The first term finds the most similar predicted transformation to each ground truth one and penalizes their differences. It can be thought of as maximizing recall in the matching and ensures that model covers all of ground truth transformations. The second term builds the opposite association and ensures precision of predictions. This bidirectional distance offers the best performance. We note that the above matching is invariant to the order of predicted parts thus allowing for non-sequential set prediction.

The second loss penalizes discrepancies between predicted part feature representations $\mathbf{r}_m^{(p)}$ and training ones $\hat{\mathbf{r}}_n^{(p)}$. In this manner the part geometry module is encouraged to predict part representations that are close to the ones produced during pre-training and that can be decoded to implicit functions according to our pretrained implicit surface decoder. Specifically, given each predicted transformation, we find its most similar training one in terms of their transformation parameters: $n' = \arg \min_n \|\hat{\theta}_n^{(p)} - \theta_m^{(p)}\|_2$. Then we penalize differences in their part feature representations:

$$\mathcal{L}_2 = \frac{1}{M} \sum_{m=1}^M \|\hat{\mathbf{r}}_{n'}^{(p)} - \mathbf{r}_m^{(p)}\|_2 \quad (4)$$

In this manner, the network is encouraged to predict part feature representations that are consistent with the ones produced during pretraining. The network is trained using a weighted sum of the losses $\mathcal{L}_1 + \lambda \mathcal{L}_2$, where λ is a hyperparameter that manages a trade-off between global part structure encoded in \mathbf{t}_m and part geometries encoded in \mathbf{r} . We set it to 0.02 in all our experiments.

In the final stage of our training (**fine-tuning**), the network is further fine-tuned to predict implicit functions that are as close as

possible to the training ones for whole shapes. Here we minimize $\mathcal{L}_{shape} = \sum_{i,p} \|(f_m(\mathbf{x}_i^{(p)}) - s_i^{(p)})\|_1$, where $s_i^{(p)}$ is the target signed distance function values of sample point $\mathbf{x}_i^{(p)} \in \mathcal{R}^3$ to the surface of the training shape p .

5 EXPERIMENTS AND RESULTS

We experiment our method in two different operational setups – part retrieval & assembly (PR&A) and implicit function assembly. The former allows constraining the parts of the estimated shape to be *exactly* like one in a shape database. The later leads to shapes whose parts are better connected to each other while also benefiting from additional training by fine-tuning the model on complete shapes. Both modes of operation are quantitatively evaluated in benchmarks where shapes are reconstructed from single RGB images or point clouds. Below we discuss datasets, evaluation metrics, comparisons of our method with state-of-the-art models and its applications.

Datasets. We use the *PartNet* dataset [Mo et al. 2019c] for our experiments, a large-scale 3D mesh dataset with semantic segmentation labels on three levels of hierarchy. For our experiments we use the three large shape categories, Tables, Chairs and Lamps (8218, 6326 and 2203 meshes respectively). For point cloud reconstruction, we train and evaluate our method and competing ones according to the PartNet provided splits, except for the comparison case of our method with JLRD [Uy et al. 2021]: in this case, we use the splits provided by authors. For comparison with part-unaware single-view reconstruction methods we also use *ShapeNetCore* [Chang et al. 2015] with same categories as PartNet. The renderings used as input on the single-view reconstruction experiments are obtained from JLRD [Uy et al. 2021] for the part-aware comparison and from DISN [Xu et al. 2019] for the part-agnostic comparison.



Fig. 5. **Qualitative point cloud reconstruction results.** Note that our model is able to reconstruct important object regions: thin stripes on chair back, curved armchair handles, swivel chair legs, etc. PQ-Net reconstructions are shown for PQ-Net-voxel version (Section 5.2).

Part extraction and preprocessing. We use part Signed Distance Fields (SDF) as supervision in our experiments. Computing those requires watertight meshes and compute those using code provided by Mescheder *et al.* [Mescheder et al. 2019] which is a modification of the code by Stutz *et al.* [Stutz and Geiger 2018]. To get watertight parts suitable for our approach, we compute convex hull/or bounding box of the part and intersect it with watertight version of the full shape. For ShapeNetCore experiments we match its shapes with our preprocessed PartNet shapes matching provided by PartNet authors. We provide more details on preprocessing in supplementary.



Fig. 6. **Part editing.** Given a query shape, users can replace or interpolate a particular part to produce a full shape with modified parts. Left shapes: original reconstruction. Right shapes: edited reconstruction.

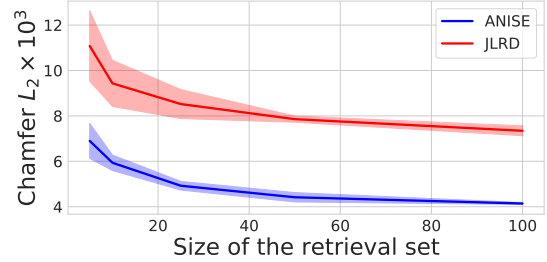


Fig. 7. **Retrieval-based SVR quality vs. size of the reference dataset.** We compare part retrieval-based (ANISE PR&A) model to shape retrieval and deformation (JLRD) approach depending on the size of retrieval dataset ($K = 5, 10, 25, 50, 100$). For each K , we perform 5 experiments and depict the mean value and standard deviation. Results are reported for Chair category.

Model training and evaluation. To obtain part code supervision, we train the part encoder-decoder on normalized parts using SDF supervision. For point cloud reconstruction, we use the PointNet implementation with residual skip connections provided by Mescheder *et al.* [Mescheder et al. 2019] and point cloud size is 2048. For single-view reconstruction we use ResNet18 as encoder for ANISE and PQ-Net; and pretrained JLRD [Uy et al. 2021] model provided by the authors. For PQ-Net, we train single view reconstruction as a regression of shape codes produced by pretrained models provided by the authors. For all experiments, we train our models with $M = 10$ part predictions. For evaluation, we use shape IoU, Chamfer distance and F-score. We reconstruct meshes from from implicit representations using marching cubes [Lorensen and Cline 1987]. Other training and evaluation details (SDF sampling, optimization, hyperparameters, F-score and IoU computations, etc.) are provided in supplementary. *We will release preprocessed data, training and evaluation code for reproducibility.*

5.1 Single view reconstruction

ANISE vs part-agnostic methods. We compare ANISE to part-agnostic single view reconstruction methods: DISN [Xu et al. 2019] and D2IM-Net [Li and Zhang 2021] in Table 1. Quantitatively, our model outperforms DISN by a large margin and performs similarly to D2IM-Net. Qualitative results (Figure 4, top) show that ANISE is better at small part accentuation but sometimes slightly incorrectly estimates proportions of the shape. Notice that the types of supervision for the methods compared here are very different. DISN and D2IM use the whole ShapeNet dataset and have access to object pose annotations. On the other hand, ANISE is only trained on PartNet categories while using their part segmentations. We believe that

Method	Chair		Table		Lamp	
	IoU (↑)	CD(↓)	IoU (↑)	CD (↓)	IoU (↑)	CD (↓)
DISN [Xu et al. 2019]	46.6	4.21	41.0	6.58	19.54	16.29
D2IM-Net [Li and Zhang 2021]	54.3	2.81	47.4	3.96	31.9	6.66
Ours (no f-tuning)	56.3	3.04	48.9	3.59	38.5	8.09

Table 1. **Comparison with part-agnostic single view reconstruction.** Our model achieves similar performance to state-of-the-art part unaware methods. IoU is computed using 64^3 resolution.

Method	Chair			Table		
	IoU (↑)	CD (↓)	F1 (↑)	IoU (↑)	CD (↓)	F1 (↑)
JLRD [Uy et al. 2021]	31.1	5.09	48.1	29.4	4.92	58.0
Ours (PR&A)	50.6	3.55	60.5	44.3	5.35	64.2
PQ-Net [Wu et al. 2020]	47.0	4.27	50.2	29.7	18.41	32.1
Ours	56.7	2.99	67.0	57.4	2.54	77.8

Table 2. **Part-aware single-view reconstruction.** Our method significantly outperforms both part-based (PQ-Net) and retrieval and deformation based (JLRD) approaches. IoU is computed using 64^3 resolution and results are multiplied by 10^2 . Chamfer distance is multiplied by 10^3 .

combining DISN and D2IM representations with ANISE might yield further performance gains for single view reconstruction.

ANISE vs. part-aware methods. We evaluate our method versus part-aware reconstruction methods: PQ-Net [Wu et al. 2020] and JLRD [Uy et al. 2021] in Table 2. ANISE outperforms both approaches in terms of volumetric (IoU) and surface-based (Chamfer) measures for Chair and Table categories. Poor performance of PQ-Net for Table category is due to the fact that it predicts extra legs that are badly positioned thus significantly increasing Chamfer distance. Qualitative analysis (Figure 4) shows that even though PQ-Net and ANISE exhibit similar priors, our model is better in recovering fine shape details.

ANISE PR&A vs. retrieval-based reconstruction. We compare our PR&A approach to a deformation and retrieval-based approach (JLRD). Our approach outperforms it by a significant margin (see Table 2). We demonstrate this in additional experiment where we limit size of the retrieval database to a certain size K (see Figure 7). PR&A based reconstruction achieves the same performance as JLRD with a reference dataset of only 5 shapes.

5.2 Point cloud reconstruction

ANISE vs part-aware methods. We compare our approach with part-aware PQ-Net [Wu et al. 2020] that utilizes sequential part assembly. Since original model was trained on voxel grids of size 64, we train a separate model that regresses PQ-Net representations from point clouds (PQ-Net-regression). This regression model follows the same point cloud network architecture employed by ANISE. Our approach clearly outperforms PQ-Net even when compared to their original voxel encoding approach (PQ-Net-voxel in Table 3), both quantitatively (Table 3) and qualitatively (Figure 5).

Part editing and constrained shape assembly. Using transformations and part codes predicted by our model, we can also constrain the shape assembly to parts from a small database. This is done by replacing the predicted part codes with closest one in the

Method	Chair		Table	
	IoU (↑)	Chamfer (↓)	IoU (↑)	Chamfer (↓)
PQ-Net-voxel [Wu et al. 2020]	67.3	3.38	47.4	5.49
PQ-Net-regression [Wu et al. 2020]	49.0	2.12	31.2	7.61
Ours	69.8	1.76	72.7	2.35

Table 3. **Part-aware point cloud reconstruction results.** IoU is computed using 64^3 resolution and results are multiplied by 10^2 . Chamfer distance is multiplied by 10^3 .

Cond. pred.	Finetuning	IOU (↑)	Chamfer (↓)	F-score(↑)
-	-	64.4	2.81	57.4
✓	-	61.4	2.44	62.0
✓	✓	70.9	1.69	73.9

Table 4. **Ablation.** Results are based on Chair category experiments for point cloud reconstruction. IoU and F-score are multiplied by 10^2 , Chamfer distance is multiplied by 10^3 .

database. In Figure 3, we illustrate this application with an example where only the parts from 5 reference shapes are used to perform point cloud reconstruction. Model correctly guesses the shape structure and selects the appropriate parts from reference shapes. In Figure 6 we also demonstrate part editing capabilities of our model through modification of the part codes.

Ablation study. Justifications for the design choices in ANISE are summarized in Table 4. Part geometry prediction conditioned on part transformations (“Cond. pred.” column) significantly outperforms its unconditional counterpart. Furthermore, supervision from SDF of fully assembled shapes gives significant boost to reconstruction quality according to all evaluated metrics (“Fine-tuning” column). We provide qualitative ablation of fine-tuning and study of failure cases in the supplementary.

6 CONCLUSION

We presented a novel shape reconstruction model formulated as an assembly of a set of neural implicits. Our network first predicts part-specific transformations which are then associated with part codes that encode geometry. After that, parts have their geometry decoded and transformed to assemble the final shape. We show that our model outperforms part-agnostic and sequential assembly models. We demonstrate its useful applications: single-view and point cloud reconstruction, selective editing of parts of reconstructed shapes, and reconstruction based on part retrieval.

Some aspects worth investigating are described as follows. Currently, our model requires pre-training of category-specific part representations which might be impractical in many scenarios. Exploring how to learn generic part codes, suitable to multiple shape categories, is left as future work. Our part transformations are currently limited: we only explore part positioning and uniform scaling. While we achieve state-of-art-results compared to other part-aware approaches, we believe adding other transformations (e.g. free-form deformations) are interesting topics for further investigation.

REFERENCES

- Sean Bell and Kavita Bala. 2015. Learning Visual Similarity for Product Design with Convolutional Neural Networks. *ACM Trans. Graph.* (July 2015).
- Rohan Chabra, Jan E. Lenssen, Eddy Ilg, Tanner Schmidt, Julian Straub, Steven Lovegrove, and Richard Newcombe. 2020. Deep Local Shapes: Learning Local SDF Priors for Detailed 3D Reconstruction. In *Eur. Conf. Comput. Vis.*
- Angel X. Chang, Thomas Funkhouser, Leonidas Guibas, Pat Hanrahan, Qixing Huang, Zimo Li, Silvio Savarese, Manolis Savva, Shuran Song, Hao Su, Jianxiong Xiao, Li Yi, and Fisher Yu. 2015. *ShapeNet: An Information-Rich 3D Model Repository*. Technical Report arXiv:1512.03012 [cs.GR].
- Siddhartha Chaudhuri, Evangelos Kalogerakis, Leonidas Guibas, and Vladlen Koltun. 2011. Probabilistic Reasoning for Assembly-Based 3D Modeling. In *ACM Trans. Graph.*
- Zhiqin Chen, Andrea Tagliasacchi, and Hao Zhang. 2020. BSP-Net: Generating compact meshes via binary space partitioning. In *CVPR*.
- Zhiqin Chen and Hao Zhang. 2019. Learning implicit fields for generative shape modeling. In *Proceedings of the IEEE/CVF Conference on Computer Vision and Pattern Recognition*. 5939–5948.
- Boyang Deng, Kyle Genova, Soroosh Yazdani, Sofien Bouaziz, Geoffrey Hinton, and Andrea Tagliasacchi. 2020. CvxNet: Learnable Convex Decomposition. In *IEEE Conf. Comput. Vis. Pattern Recog.*
- Anastasia Dubrovina, Fei Xia, Panos Achlioptas, Mira Shalah, Raphael Groscore, and Leonidas J. Guibas. 2019. Composite Shape Modeling via Latent Space Factorization. In *Proceedings of the IEEE/CVF International Conference on Computer Vision (ICCV)*.
- Thomas Funkhouser, Michael Kazhdan, Philip Shilane, Patrick Min, William Kiefer, Ayellet Tal, Szymon Rusinkiewicz, and David Dobkin. 2004. Modeling by example. *ACM Trans. Graph.* (2004).
- Matheus Gadelha, Giorgio Gori, Duygu Ceylan, Radomir Mech, Nathan Carr, Tamy Boubekeur, Rui Wang, and Subhansu Maji. 2020. Learning Generative Models of Shape Handles. In *IEEE Conf. Comput. Vis. Pattern Recog.*
- Kyle Genova, Forrester Cole, Avneesh Sud, Aaron Sarna, and Thomas Funkhouser. 2020. Local deep implicit functions for 3d shape. In *Proceedings of the IEEE/CVF Conference on Computer Vision and Pattern Recognition*. 4857–4866.
- Kyle Genova, Forrester Cole, Daniel Vlasic, Aaron Sarna, William T Freeman, and Thomas Funkhouser. 2019. Learning shape templates with structured implicit functions. In *Proceedings of the IEEE/CVF International Conference on Computer Vision*. 7154–7164.
- Chiyu Max Jiang, Avneesh Sud, Ameesh Makadia, Jingwei Huang, Matthias Nießner, and Thomas Funkhouser. 2020. Local Implicit Grid Representations for 3D Scenes. In *IEEE Conf. Comput. Vis. Pattern Recog.*
- Evangelos Kalogerakis, Siddhartha Chaudhuri, Daphne Koller, and Vladlen Koltun. 2012. A Probabilistic Model of Component-Based Shape Synthesis. *ACM Trans. Graph.* (2012).
- Jun Li, Chengjie Niu, and Kai Xu. 2020. Learning part generation and assembly for structure-aware shape synthesis. In *Proceedings of the AAAI Conference on Artificial Intelligence*, Vol. 34. 11362–11369.
- Jun Li, Kai Xu, Siddhartha Chaudhuri, Ersin Yumer, Hao Zhang, and Leonidas Guibas. 2017. GRASS: Generative Recursive Autoencoders for Shape Structures. *ACM Trans. Graph.* (2017).
- Manyi Li and Hao Zhang. 2021. D2im-net: Learning detail disentangled implicit fields from single images. In *Proceedings of the IEEE/CVF Conference on Computer Vision and Pattern Recognition*. 10246–10255.
- Yangyan Li, Hao Su, Charles Ruizhongtai Qi, Noa Fish, Daniel Cohen-Or, and Leonidas J. Guibas. 2015. Joint Embeddings of Shapes and Images via CNN Image Purification. *ACM Trans. Graph.* (2015).
- Gidi Littwin and Lior Wolf. 2019. Deep Meta Functionals for Shape Representation. In *Int. Conf. Comput. Vis.*, Vol. abs/1908.06277.
- William E Lorensen and Harvey E Cline. 1987. Marching cubes: A high resolution 3D surface construction algorithm. *ACM siggraph computer graphics* 21, 4 (1987), 163–169.
- Lars Mescheder, Michael Oechsle, Michael Niemeyer, Sebastian Nowozin, and Andreas Geiger. 2019. Occupancy networks: Learning 3d reconstruction in function space. In *IEEE Conf. Comput. Vis. Pattern Recog.*
- Kaichun Mo, Paul Guerrero, Li Yi, Hao Su, Peter Wonka, Niloy Mitra, and Leonidas Guibas. 2019a. StructureNet: Hierarchical Graph Networks for 3D Shape Generation. *ACM Trans. Graph.* (2019).
- Kaichun Mo, Shilin Zhu, Angel X Chang, Li Yi, Subarna Tripathi, Leonidas J Guibas, and Hao Su. 2019b. Partnet: A large-scale benchmark for fine-grained and hierarchical part-level 3d object understanding. In *IEEE Conf. Comput. Vis. Pattern Recog.*
- Kaichun Mo, Shilin Zhu, Angel X Chang, Li Yi, Subarna Tripathi, Leonidas J Guibas, and Hao Su. 2019c. Partnet: A large-scale benchmark for fine-grained and hierarchical part-level 3d object understanding. In *Proceedings of the IEEE/CVF Conference on Computer Vision and Pattern Recognition*. 909–918.
- Ken Muse, David E. Breen, Ross T. Whitaker, and Alan H. Barr. 2002. Level Set Surface Editing Operators. *ACM Trans. Graph.* 21, 3 (2002), 330–338.
- Liangliang Nan, Ke Xie, and Andrei Sharf. 2012. A Search-Classify Approach for Cluttered Indoor Scene Understanding. *ACM Trans. Graph.* (2012).
- Jeong Joon Park, Peter Florence, Julian Straub, Richard Newcombe, and Steven Lovegrove. 2019. DeepSDF: Learning Continuous Signed Distance Functions for Shape Representation. In *IEEE Conf. Comput. Vis. Pattern Recog.*
- Despoina Paschalidou, Angelos Katharopoulos, Andreas Geiger, and Sanja Fidler. 2021. Neural Parts: Learning Expressive 3D Shape Abstractions with Invertible Neural Networks. In *IEEE Conf. Comput. Vis. Pattern Recog.*
- Songyou Peng, Michael Niemeyer, Lars Mescheder, Marc Pollefeys, and Andreas Geiger. 2020. Convolutional Occupancy Networks. In *Eur. Conf. Comput. Vis.*
- Charles R Qi, Hao Su, Kaichun Mo, and Leonidas J Guibas. 2017. Pointnet: Deep learning on point sets for 3d classification and segmentation. In *Proceedings of the IEEE conference on computer vision and pattern recognition*. 652–660.
- Tim Reiner, Gregor Mückl, and Carsten Dachsbacher. 2011. Interactive Modeling of Implicit Surfaces Using a Direct Visualization Approach with Signed Distance Functions. *Comput. Graph.* 35, 3 (2011).
- Adriana Schulz, Ariel Shamir, Ilya Baran, David I. W. Levin, Pitchaya Sitthi-Amorn, and Wojciech Matusik. 2017. Retrieval on Parametric Shape Collections. *ACM Trans. Graph.* (2017).
- David Stutz and Andreas Geiger. 2018. Learning 3d shape completion from laser scan data with weak supervision. In *IEEE Conf. Comput. Vis. Pattern Recog.* 1955–1964.
- Mikaela Angelina Uy, Vladimir G. Kim, Minhyuk Sung, Noam Aigerman, Siddhartha Chaudhuri, and Leonidas Guibas. 2021. Joint Learning of 3D Shape Retrieval and Deformation.
- Rundi Wu, Yixin Zhuang, Kai Xu, Hao Zhang, and Baoquan Chen. 2020. Pq-net: A generative part seq2seq network for 3d shapes. In *IEEE Conf. Comput. Vis. Pattern Recog.*
- Kai Xu, Hao Zhang, Daniel Cohen-Or, and Baoquan Chen. 2012. Fit and Diverse: Set Evolution for Inspiring 3D Shape Galleries. *ACM Trans. Graph.* (2012).
- Qiangeng Xu, Weiye Wang, Duygu Ceylan, Radomir Mech, and Ulrich Neumann. 2019. DISN: Deep Implicit Surface Network for High-quality Single-view 3D Reconstruction. In *Adv. Neural Inform. Process. Syst.*
- Chuhang Zou, Ersin Yumer, Jimei Yang, Duygu Ceylan, and Derek Hoiem. 2017. 3d-prnn: Generating shape primitives with recurrent neural networks. In *Int. Conf. Comput. Vis.*